Latin American Journal of Solids and Structures
www.lajss.org

Experimental Evaluation of Low-Pass Shock Isolation Performance of Elastomers Using Frequency-Based Kolsky Bar Analyses

Abstract

Elastomeric materials are used as shock isolation materials in a variety of environments to dampen vibrations and/or absorb energy from external impact for minimizing energy transfer between two objects or bodies. Some applications require the shock isolation materials to behave as a low-pass mechanical filter to mitigate the shock/impact at high frequencies but transmit the energy at low frequencies with minimal attenuation. In order to fulfill this requirement, a shock isolation material needs to be carefully evaluated and selected with proper experimental design, procedures, and analyses. In this study, a Kolsky bar was modified with pre-compression (up to 15.5 kN) and confinement capabilities to evaluate low-pass shock isolation performance in terms of acceleration attenuation through a variety of elastomers. The effects of preload and specimen geometry on the low-pass shock isolation response were also investigated.

Keywords

Shock isolation, frequency response, Kolsky bar, rubbers, EPDM, polyurethane, neoprene

Brett Sanborn [a]
Bo Song [a]
Erik Nishida [a]
Marlene Knight [a]

[a] Sandia National Laboratories, Albuquerque, NM 87185, USA.
bsanbor@sandia.gov, bsong@sandia.gov, eenishi@sandia.gov, mechave@sandia.gov

http://dx.doi.org/10.1590/1679-78253268

Received 02.08.2016
In revised form 04.01.2017
Accepted 22.01.2017
Available online 26.01.2017

1 INTRODUCTION

Shock isolation is an essential concept in component design to mitigate or isolate external shock/impact energy from internal sensitive sub-component devices. Appropriate materials or systems need to be carefully designed or selected for effective and efficient shock isolation. An excellent shock isolation material should be capable of absorbing external shock/impact energy and attenuating acceleration when subjected to impact/shock loading. While a variety of materials such as glass microbeads can be used for shock isolation (Yoon and Kim 2006), elastomers have been widely used as shock isolation materials due to their superior flexibility associated with excellent energy absorption and vibration damping capabilities. However, the shock isolation performance of elastomers

varies in applications depending on intrinsic mechanical properties, geometries, dimensions, assembly process, and specific requirements. One example requirement may refer to frequencies. In most applications, high frequencies, which are a typical phenomena in shock or impact environments (Lalanne 2009), are unfavorable and need to be mitigated in order to protect sensitive components. When a shock isolation material is applied to mitigate the high frequencies, the low frequencies are dampened as well such that the internal components or sensors are not isolated too much to correctly sense and respond to actual shock or impact loading. In such specific applications, the shock isolation materials are desired to isolate high frequencies only but allow low frequencies to pass through with minimal attenuation.

Effectiveness of elastomers as mechanical low-pass filters has been investigated extensively as shock isolators for accelerometers. In one application, a polymer material was chosen as a low-pass isolation material to protect accelerometers up to a frequency of 15 kHz (Chu 1988). In another scheme, Bateman et al. (Bateman et al. 1990) installed an accelerometer between two polysulfide rubber pads in an attempt to retain accelerometer fidelity up to 10 kHz and tried to prevent high frequencies above 10 kHz from reaching the accelerometer. Yiannakopoulos and van der Schaaf (Yiannakopoulos and van der Schaaf 1998) evaluated a mix of commercially available and novel arrangements to protect piezoresistive and piezoelectric accelerometers using silicone, butyl, and bromo-butyl rubber from frequencies ranging between 8-10 kHz. The deformation, strain rate, and frequencies which the materials are subjected to in conventional DMA or vibration methods are significantly lower than those in shock or impact environments. Therefore, a new low-pass experimental evaluation method needs to be developed to subject the material to larger deformation, higher strain rates and frequencies.

Elastomers used in shock or vibration isolators are routinely confined and subjected to preload during assembly process. The confinement subjects the elastomers to multiple stress states or a nearly uniaxial strain state. The dynamic responses of foam materials and elastomers, typically used for shock or impact isolation applications, have been found drastically different when the state changes from uniaxial stress to unaxial strain (Song and Chen 2004, Song et al. 2005). Such mechanical property changes are expected to change the shock or impact isolation performance (Nelson 1996). In addition, due to nonlinear mechanical response, the preload changes the initial stress state of the elastomers and consequently influences their shock or impact isolation performance (Thorin et al. 2012) in applications ranging from the electronics industry to protect computer hard drives (Park et al. 2012) to automotive industry engine mounts (Cardillo 1964) to civil structural applications for seismic isolation of buildings (Zou et al. 2011).

To evaluate the shock isolation performance of a specific material, transmitted acceleration is usually used as the dominating parameter for performance (Mercer and Rees 1971, Landro et al. 2002, DeMarco et al. 2010). Typical evaluation experiments involve placing accelerometers on the opposite side to the impact of the material or component to directly measure the transmitted acceleration (Landro et al. 2002, DeMarco et al. 2010). However, this time-domain analysis was very limited to evaluate the frequency bandwidth with respect to shock isolation performance. A Kolsky compression bar (also called split Hopkinson pressure bar, SHPB) has been recently employed to characterize the frequency response of shock mitigation of a polymethylene diisocyanate (PMDI) based rigid polyurethane foam (Song and Nelson 2015). The PMDI foam material showed excellent

shock mitigation capability: nearly all shock energy at frequencies higher than 1.5 kHz was absorbed. Shock energies at frequencies lower than 1.5 kHz were also absorbed; however, the energy dissipation below 1.5 kHz was diminished to about 80%, which indicates that about 20% of the energy below 1.5 kHz is transmitted through the material. Such an amount of energy dissipation resulted in significant attenuation of transmitted acceleration from low to high frequencies. In another study, silicone foam was subjected to small amounts of pre-strain and the energy dissipation behavior in the frequency domain was investigated (Sanborn et al. 2016). For the silicone foam, all of the impact energy was absorbed across the entire frequency range. Therefore, both PMDI and silicone foams have been demonstrated to be capable of mitigating shock or impact energy but not good candidates for low-pass shock isolation applications.

In this study, a pre-compression load capability up to 15.5 kN was developed for a Kolsky compression bar for low-pass shock isolation performance evaluation of three different elastomers passively confined with a snug-fit tube. A previously developed (Song and Nelson 2015) frequency-based analysis on Kolsky bar experiments was used to analyze the low-pass shock isolation response, in terms of transmitted accelerations, of a variety of elastomers with different geometrical and loading conditions.

2 MATERIALS AND SPECIMENS

In this study, polyurethane, neoprene, and ethylene propylene diene monomer (EPDM) with different hardness were characterized and evaluated for low-pass shock isolation performance. The material and specimen information used in this study is summarized in Table 1. The Shore A durometer of polyurethane, neoprene, and EPDM, were 80A, 70A, and 60A, and had densities of 1233 ± 7.37 kg/m^3, 1159 ± 22.7 kg/m^3, 1321.5 ± 3.9 kg/m^3, respectively. Each material was made into cylindrical specimens with different diameters of 25.4 mm (the same diameter as the pressure bars), 19.05 mm, 15.88 mm, and 9.53 mm. Specimen thickness for polyurethane, neoprene, and EPDM were 3.08 mm, 2.97 mm, and 3.10 mm, respectively.

Material	Density (kg/m^3)	Durometer (Shore A)	Thickness (mm)	Diameter (mm)
Polyurethane	1233 ± 7.4	80	3.08	25.4, 19.05, 15.88, 9.53
Neoprene	1159 ± 22.7	70	2.97	25.4, 19.05, 15.88, 9.53
EPDM	1321.5 ± 3.9	60	3.10	25.4, 19.05, 15.88, 9.53

Table 1: Materials and specimen geometries.

For Neoprene and EPDM rubber, one experiment at each diameter was conducted. To check repeatability of the acceleration transmission behavior for polyurethane rubber, two experiments at each diameter were conducted.

3 EXPERIMENTAL SETUP

In a conventional Kolsky compression bar setup, a striker is launched from a gas gun and impacts the end of the incident bar. The impact produces a stress pulse that propagates along the incident

bar. When the stress pulse arrives at the specimen sandwiched between the incident and transmission bars, part of the incident pulse is reflected back into the incident bar and the rest transmits through the specimen into the transmission bar. Strain gages mounted on the incident and transmission bars are used to provide the time domain load and deformation histories from which the frequency domain behavior can be derived through Fourier transform. The strain gage signal was acquired with a Teledyne LeCroy HDO8058 high definition oscilloscope at a sampling rate of 50 MHz.

The incident bar used in this study was 3657 mm long while the transmission bar was 2134 mm long. Incident and transmission strain gages were located 1915 mm and 762 mm from the gage section, respectively. The bar material is C300 maraging steel that had a Young's modulus of approximately 190 GPa and elastic wave speed of 4870 m/s. In addition, the Kolsky compression bar was modified to accommodate pre-compression capabilities up to 15.5 kN to investigate the effect of preload on the shock isolation response of different materials. A hydraulic jack was applied to the free end of the transmission bar to facilitate a preload of up to 15.5 kN on the system, as shown in Fig. 1. While hydraulic jacks have been used to generate impact in previous studies (Zhao and Gary 1997, Othman and Gary 2007), the goal in the present study is to facilitate a static preload. As shown in the schematic in Fig. 1, a reaction plate and platen were placed at the impact end of the compression bar to prevent the system from moving toward the striker when the hydraulic pressure is applied to the transmission bar end. Four tie rods, which prevent any buckling in the bars (Frew et al. 2010), were connected between the reaction plate and jack fixture to accommodate the pre-compression load from possible buckling of the bars and fixtures when subjected to such a high-amplitude preload. The platen at the impact end is free to move in the impact direction but prevents the incident bar from moving away from the jack (the opposite direction to the impact), similar to the setup described by Chen and Song (Chen and Song 2010) for high triaxial loads. This configuration allows the bar system to move only along the dynamic loading direction. In this study, the bar system including the specimen was subjected to a static pre-compression load of 15.5 kN (3500 lbf) before dynamic loading.

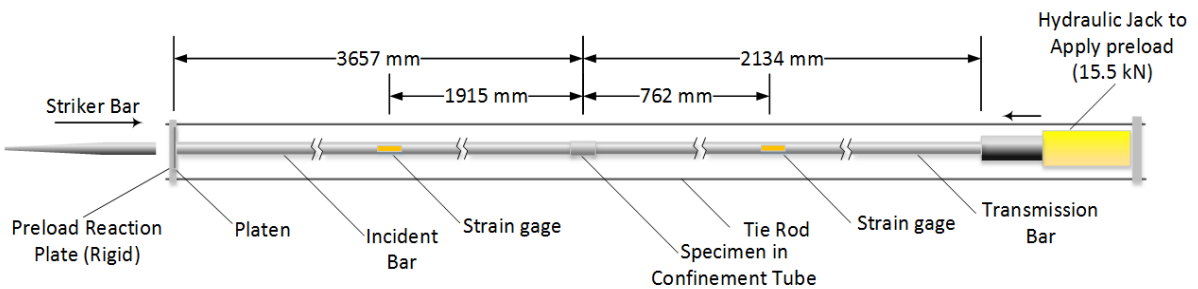

Figure 1: Modified compression setup schematic.

Before the static pre-compression load is applied, the thickness of the specimen was carefully measured and used to preset a gap between the incident and transmission bars to prevent any unexpected additional pre-compression on the specimen, particularly when the specimen material is soft, during specimen installation procedure. After the specimen was inserted into the gap, a steel

confinement tube was slid over the specimen as shown in Fig. 2. The 4340 steel tube that confined the specimen in the radial direction had dimensions of 31.8 mm for the outer diameter, 25.5 mm for the inner diameter, and a length of 50.83 mm. After the specimen was placed between the bars and the confinement tube was slid over the specimen, the preload was applied and the load of 15.5 kN was verified using the strain gage measurements on the pressure bars. In general, a couple of minutes spanned between application of the static pre-compression load and dynamic loading. No creep of the sample was observed between the preload and dynamic loading. The pre-compression strain generated in the specimen subjected to static pre-compression load was not directly measured. However, it is imagined the pre-compression strain varied with different specimen material and diameter. The varying pre-compression strains are expected to result in different low-pass shock isolation performance, due to nonlinear rate-dependent stress-strain response of elastomers (Song and Chen 2003, Song and Chen 2004).

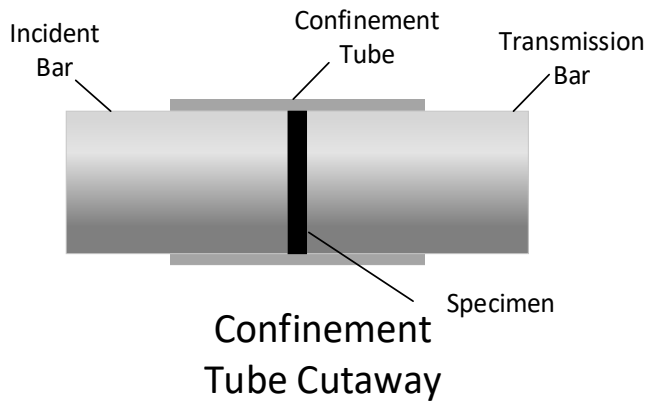

Figure 2: Schematic of specimen under triaxial confinement inside the steel tube.

To capture the response of the material over a wide range of frequencies, a tapered striker as shown in Fig. 3 was used to generate a uniquely shaped incident pulse. Though tapered strikers have been used in the past to achieve altered loading pulses for rock materials (Li et al. 2000, Zhou et al. 2012, Kumar et al. 2004, Kobayashi et al. 2000), the application here is to alter the frequency content and unloading behavior in the incident pulse by using the tapered end as the tail of the striker rather than the impact end (Fig. 3). It is noted that no pulse shaping or grease was used to alter the loading profile because using pulse shapers or grease would cut off the high-frequency content of the incident pulse. A fast rise time is generated by the straight portion of the higher impedance striker impacting the lower impedance incident bar. The tapered tail of the tungsten striker created a smooth unloading profile on the incident pulse instead of the typical step-wise unloading profile created by the impact of a higher impedance tungsten striker on the steel incident bar (Song et al. 2009). The incident pulse, which is discussed in the Results and Discussion section, has been shown to contain a wider range of frequencies, especially in the high frequency regime due to the fast rise time and long unloading tail compared to the pulse generated by a conventional cylindrical striker (Sanborn et al. 2016). This extended frequency range helps elucidate the frequency response of different shock isolation materials.

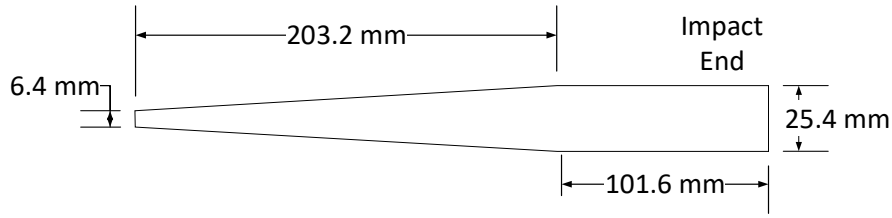

Figure 3: Sketch of the tapered striker.

Based on the incident, reflected, and transmitted time-domain strain pulses, the acceleration applied to the specimen can be used to evaluate the shock isolation potential of a material. The input acceleration is calculated using (Song and Nelson 2015) the input velocity, V_{input}

$$a_{input}(t) = \frac{dV_{input}(t)}{dt} = C_0 \frac{d(\varepsilon_i(t) - \varepsilon_r(t))}{dt} = a_i(t) - a_r(t) \tag{1}$$

where ε_i and ε_r are the incident and reflected strain pulses, respectively; $a_i(t)$ and $a_r(t)$ are the corresponding acceleration time histories, respectively; and C_0 is the wave speed of the bar material. The corresponding output acceleration is calculated using the transmitted velocity, V_t, as

$$a_{Output}(t) = \frac{dV_t(t)}{dt} = C_0 \frac{d\varepsilon_t(t)}{dt} = a_t(t) \tag{2}$$

where ε_t is the transmitted strain pulse and $a_t(t)$ is the transmitted acceleration time history. It is noted here that equations (1) and (2) can be used with or without static preload. Each time-domain acceleration history *a(t)* derived from each of the signals has a Fourier transform

$$\hat{a}(f) = \int_{-\infty}^{+\infty} a(t) e^{-2i\pi f t} dt \tag{3}$$

where f is the frequency. Thus, the acceleration transmission ratio, δ_{AT}, through the specimen can be calculated using the frequency spectra of the input and output accelerations as

$$\delta_{AT}(f) = \frac{|\widehat{a_t}(f)|}{|\widehat{a_i}(f) - \widehat{a_r}(f)|} \tag{4}$$

This represents the acceleration transmission through the sample as a function of frequency. Although differentiating to calculate the acceleration can generate noise in the signal, such noise is at a high frequency which is well above 500 kHz (Song and Nelson 2015), so any noise generated through differentiation calculation should not affect our investigation. In addition, the wave dispersion correction is not necessary to considered when conducting frequency-domain analysis (Eq. (4)) (Song and Nelson 2015).

4 RESULTS AND DISCUSSION

The experimental setup described in this study has similar challenges to dynamic experiments with triaxial confinement described by Chen and Song (Chen and Song 2011). Chen and Song described

that, upon impact of the striker and after the unloading portion of the incident pulse, the incident signal approaches a negative value, corresponding to tension in the incident bar. Figure 4 shows a plot of the original strain signals collected, in this study, during a dynamic experiment on polyurethane rubber preloaded to 15.5 kN, where the striker speed was 13 m/s. Since a static pre-compression load of 15.5 kN was applied to the system to compress the specimen prior to dynamic loading, and taking compression to be positive, the incident and transmission bar strain gages would have a positive offset of approximately 170 microstrain after the pre-compression load phase of the experiment. However, the incident and transmission bar strain gages were set to zero following the application of the preload. Figure 4 shows that the incident pulse approaches a negative value after unloading. This apparent "negative" behavior in the incident pulse was caused by the incident bar losing the static axial load after the striker impact occurred due to the transfer of the free boundary condition from the free end of the striker to the incident bar. The transmitted pulse is apparently not affected by the loss in preload force as the baseline of the transmitted pulse in Fig. 4 remains at zero prior to the arrival of the pulse. According to Fig. 4, the preload on the incident bar resumes at a time of 400 µs since the baseline of the incident pulse returns to zero at that time. This is caused by the release of previously stored energy by static pre-compression load. The unloading of the first dynamic compressive loading released the dynamic compressive energy only but left a temporary free boundary condition at the impact end. Therefore, the previously stored static pre-compression energy moves the incident bar back to make the platen contact with the preload reaction plate again. This means that the system was recovered back to original static pre-compression status, moving the baseline back to zero. In order to demonstrate the effect of preload on the incident pulse, a comparison of time-domain incident pulses generated by the same tapered striker but at 0 and 15.5 kN preloads was performed and shown in Fig. 5. Figure 5 clearly shows that, though the rise time and peak strain of the incident pulses are identical and follow nearly the same unloading behavior until about 125 µs, when the incident pulse from the preloaded experiment becomes negative due to the preload in the system.

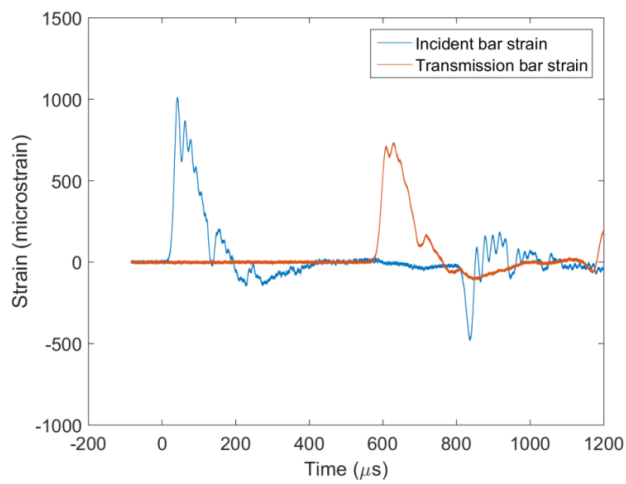

Figure 4: Original experimental record from an experiment on preloaded polyurethane rubber.

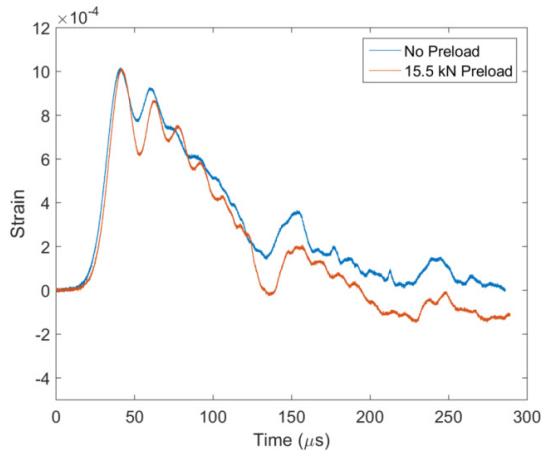

Figure 5: Incident pulses generated using the tapered striker for non-preloaded and preloaded experiments.

It is noted that the constant quasi-static pre-compression load offsets the baseline of the bar strain signals, which represent the velocity histories associated with the incident and reflected pulses. However, the constant offset in the particle velocities should not influence the incident and reflected acceleration histories through differentiation.

The input and output accelerations in the time domain through a polyurethane specimen were calculated using Equations (1) and (2) and are shown in Fig. 6. In the time domain, the input acceleration had a peak value of 450,000 G while the output acceleration had peak amplitude of 180,000 G, indicating that the polyurethane material transmitted 40% of the acceleration. It should be noted that wave dispersion occurs in the time-domain acceleration calculations. However, the effect of wave dispersion will be eliminated in the frequency domain analysis.

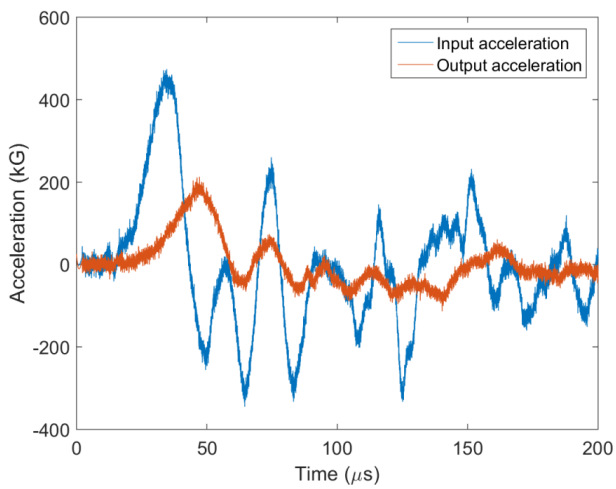

Figure 6: Input and output accelerations through a polyurethane specimen.

The corresponding input and output acceleration behavior in the frequency domain is calculated with Eq. (4) and shown in Fig. 7a. According to the acceleration transmission profile for this polyu-

rethane 80A experiment shown in Fig. 7, the output acceleration is very close but slightly higher than the input acceleration at the frequencies below 0.6 kHz, which is zoomed in and shown in Fig. 7b. This generates an acceleration transmission coefficient above 1 at low frequencies, as shown in Fig. 8. In this case, the polyurethane 80A specimen was stiffened due to the high amplitude (15.5 kN) of the pre-compression load before dynamic loading. This highly stiffened specimen may generate a high amplitude of recovery force when the specimen is unloaded. The unloading/recovery force therefore pushed the incident and transmission bars away, which decelerated the incident bar end but further accelerated the transmission bar. This will possibly result in higher amplitude of output acceleration than input acceleration, and consequently an acceleration transmission factor greater than 1. However, the greater acceleration transmission factor does not contribute to all frequencies uniformly. The output acceleration transmission factor becomes higher than the input at low frequencies (below 0.6 kHz) only. At high frequencies, the polyurethane 80A rubber dampened the acceleration, even though it was significantly stiffened before dynamic loading. Thus, it is shown in Fig. 7a that past a frequency of 0.6 kHz, the input acceleration is higher than the output acceleration.

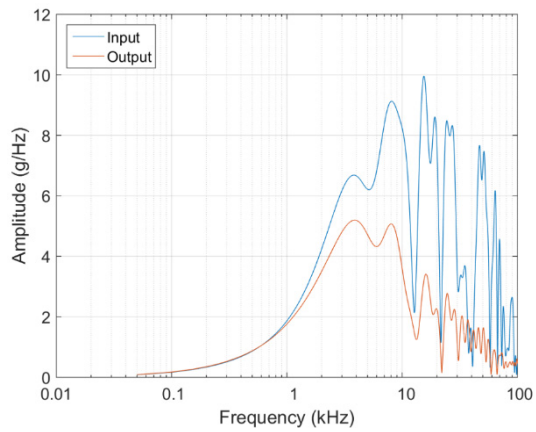

Figure 7a: Input and output acceleration transmission behavior in the frequency domain.

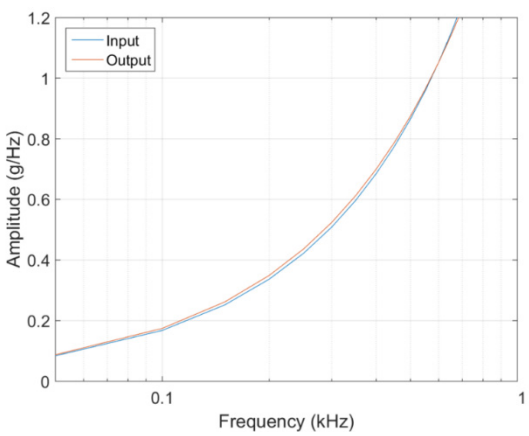

Figure 7b: Zoomed input and output acceleration transmission behavior in the frequency domain.

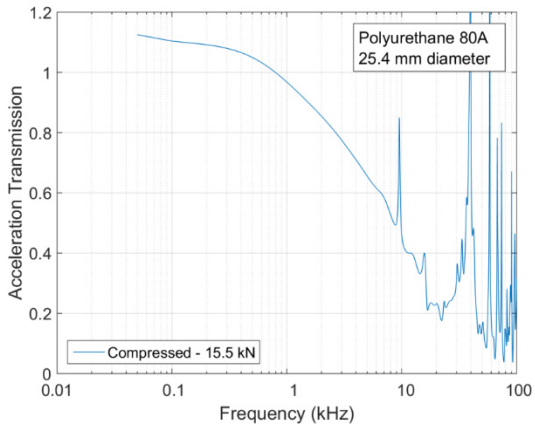

Figure 8: Acceleration transmission behavior of polyurethane pre-compressed to 15.5 kN.

The same polyurethane 80A rubber but with different initial diameters were also dynamically characterized with the same pre-compression load of 15.5 kN. The acceleration transmission characteristic in the frequency domain is summarized in Fig. 9. In Fig. 9, two experiments at each condition are provided to show the repeatability of the acceleration transmission response of the rubber. In general, the results for each initial diameter are fairly close after a frequency of about 1 kHz is reached. The results were not highly repeatable at the frequencies below 1 kHz, which may because the recovery process as mentioned earlier, or possibly by slight differences in specimen initial diameter and hence small differences in initial strain even at the same pre-compression load. However, as shown in Fig. 9, the acceleration transmission ratios for all specimens are close to 1 when the frequency is below 1 kHz. This means that the polyurethane 80A exhibits a good low-pass acceleration transmission up to 1 kHz, regardless of the specimen diameter. It is noted that, under the constant 15.5 kN pre-load, the specimen with a smaller diameter was subjected to uniaxial pre-compression until the specimen was deformed to the same diameter as the pressure bars, meaning the smaller diameter specimens reached a higher level of strain for the same amount of stress. Once the quasi-static force applied to the specimen was enough to deform the specimen to the bar diameter, the specimen was continuously subjected to a triaxial pre-compression load of 15.5 kN. The transition from uniaxial to triaxial pre-compression varied from specimens with different initial diameters. In other words, even though the same pre-compression load was applied, the stress and strain states were different in the specimens with different diameters. However, the difference in the stress and strain states in the specimens did not seem to affect the acceleration transmission ratio at the frequencies below 1 kHz. Instead, the acceleration transmission ratio at the frequencies higher than 1 kHz varied with the initial specimen diameters. The acceleration transmission ratio attenuated more as the specimen diameter increased. The low-pass cutoff frequency can be defined at different thresholds for different applications. In this study however, the low-pass frequency was defined as the frequency where the acceleration transmission ratio dropped to 0.9, or 90% acceleration transmission, represented by a dashed line in Fig. 9. As shown in Fig. 9, the low-pass frequencies for the polyurethane 80A specimens were determined as 1.43 kHz for 25.4-mm-diameter samples, 2.13 kHz for 19.05-mm-diameter samples, 2.5 kHz for 15.88-mm-diameter samples, and 10.5 kHz for 9.53-mm-diameter samples, respectively.

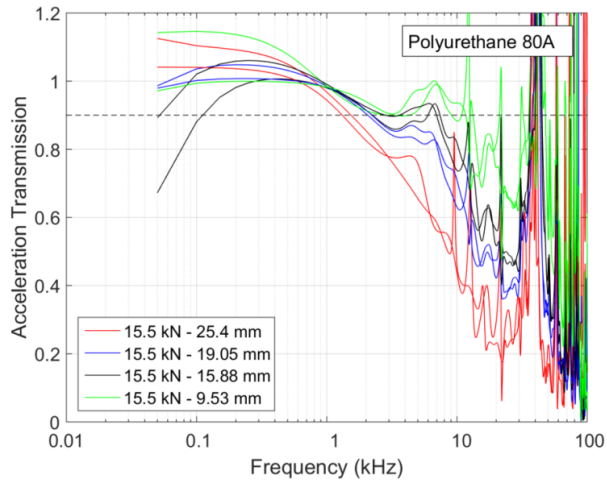

Figure 9: Acceleration transmission behavior of polyurethane rubber at different initial diameters preloaded to 15.5 kN prior to dynamic loading. Two experiments were conducted for each diameter to show repeatability. The dashed line represents the low-pass cutoff acceleration transmission of 90% defined for this study.

EPDM rubber shows a similar trend in acceleration transmission behavior with diameters under the same preload conditions. Figure 10 shows the results of acceleration transmission for the EPDM rubber specimens with different diameters, but subjected to the same pre-compression load of 15.5 kN. Similar to the polyurethane 80A rubber, the EPDM rubber had almost full acceleration transmission up to a frequency of 1 kHz, regardless of the specimen diameter. The acceleration transmission of EPDM rubber begins to fall off when the frequency becomes higher. The low-pass frequencies with the acceptance level of 90% acceleration transmission for the EPDM 60A rubber are 1.5 kHz for the 25.4-mm-diameter sample, 2.1 kHz for the 19.05-mm-diameter sample, 2.4 kHz for the 15.88-mm-diameter sample, and 2.55 kHz for the 9.53-mm-diameter sample, respectively. The effect of specimen diameter on the low-pass frequency for the EPDM 60A rubber is not as significant as that for the polyurethane 80A rubber. It should be noted that the acceleration transmission for the 9.53 mm dropped below the 90% threshold and then increased to above 90%, only to decrease again below the threshold at about 8 kHz. In this case, the first crossing of the 90% threshold was taken to be the cutoff. In other applications, the threshold could be set at a different level.

Unlike the polyurethane 80A and EPDM 60A rubbers, the neoprene 70A rubber does not exhibit significant effect of specimen diameter. Figure 11 shows that all neoprene 70A rubber specimens, even though with different diameters, have an acceleration transmission of around 1 until a frequency of about 1 kHz, which are similar to the polyurethane 80A and EPDM 60A rubbers. However, the acceleration transmission ratio drops to 0.9 at 1.8 kHz for the 25.4-mm-diameter sample, 2.1 kHz for the 19.05-mm-diameter sample, 1.65 kHz for the 15.88-mm-diameter sample, and 2.2 kHz for the 9.53-mm-diameter sample, showing a negligible effect of specimen diameter on low-pass frequency.

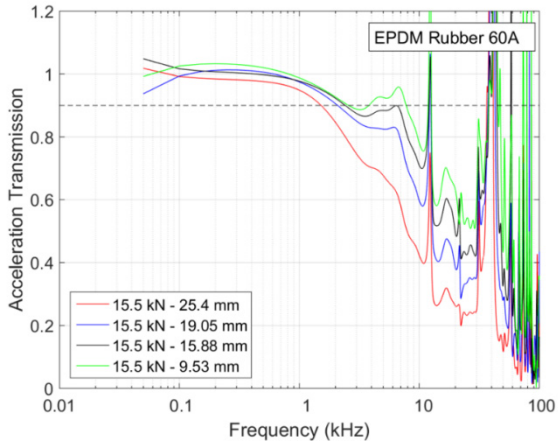

Figure 10: EPDM rubber acceleration transmission behavior as a function of specimen diameter under a preload of 15.5 kN. The dashed line represents the low-pass cutoff acceleration transmission of 90% defined for this study.

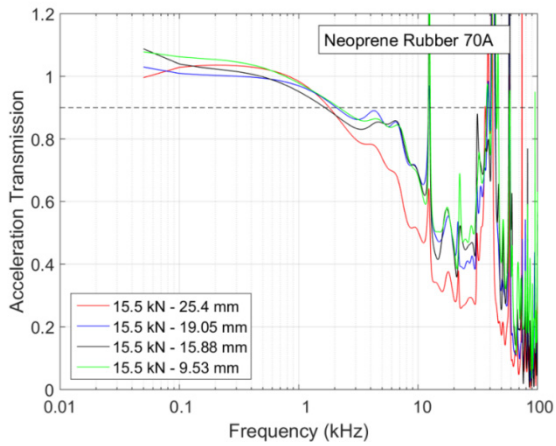

Figure 11: Acceleration transmission response of neoprene rubber at different diameters. The dashed line represents the low-pass cutoff acceleration transmission of 90% defined for this study.

Figure 12 summarizes the effect of specimen diameter on the low-pass cutoff frequency for the three rubber materials. The polyurethane 80A rubber exhibits the most significant effect of specimen diameter; whereas the Neoprene 70A rubber shows no effect of specimen diameter. Such a difference may be caused by the different intrinsic material response for the three materials since the specimen geometries and dimensions are very close for the three materials. As mentioned earlier, the specimens were subjected to uniaxial pre-compression load (except for specimens that had the same diameter as the bars) and then followed by triaxial pre-compression load (due to the steel tube). Therefore, after the same pre-compression load was applied, the specimens ended up with different stress and strain states, which would consequently affect the low-pass frequency response. In the future, an effort will be made to quantify the exact state of stress and strain following pre-compression prior to impact loading using a combination of experimental and computational methods.

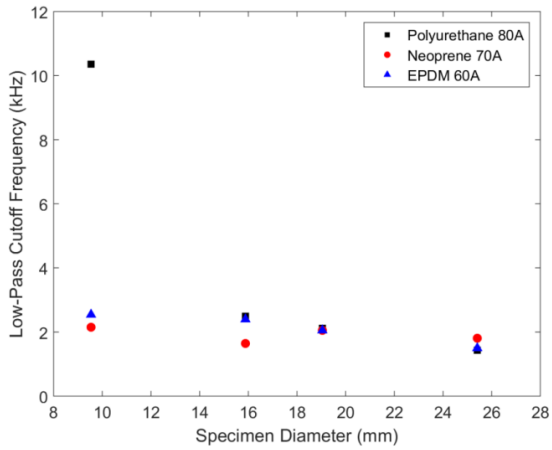

Figure 12: Effect of specimen diameter on low-pass cutoff frequency.

In order to understand the effect of intrinsic stress-strain response on the low-pass frequency with respect to acceleration transmission, future work must be conducted to characterize the dynamic stress-strain response under different loading rates and stress states for the materials presented here. For example, the compressive stress-strain curves of the materials with and without confinement would be required to understand the transition from uniaxial stress and triaxial stress state, the nonlinear hardening state of the materials during pre-compression load, and the high-rate triaxial hardening behavior, including dynamic bulk and shear moduli, of the materials during impact loading. Since the mechanical response of rubbers is highly temperature dependent, experiments over a wide range of temperatures may be needed to describe the low-pass frequency response of elastomers for different environmental applications.

5 CONCLUSIONS

A Kolsky compression bar was modified to statically preload elastomer specimens prior to dynamic loading to evaluate the shock isolation capabilities under impact loading of different materials. A new preload and confinement setup was presented that utilized a hydraulic jack, tie rods, and a steel tube to provide passive confinement of rubber specimens under axial preloads up to 15.5 kN. A tapered striker was designed to produce a pulse with a fast rise time and long unloading tail to subject the polyurethane 80A, neoprene 70A, and EPDM 60A rubbers of different diameters to a wide range of input frequencies. The time-domain strain gage measurements on the pressure bars were converted into the frequency domain by FFT to investigate the acceleration transmission behavior for the different materials. The cutoff frequencies with 90% acceleration transmission of the polyurethane 80A and EPDM 60A rubber increased with decreasing specimen diameter. The cutoff frequency of the neoprene 70A rubber had a common drop-off frequency of about 2 kHz, regardless of specimen diameter. The methods described here can be used for design of shock isolation systems. Experiments can be carried out at specific preload levels for different candidate materials to select the best material for different isolation or low-pass frequency transmission under impact conditions.

The results presented here for the polyurethane 80A, neoprene 70A, and EPDM 60A rubbers are only applicable for the specific preload, specimen thickness, diameter, and striker velocity of 13 m/s.

Acknowledgments

Sandia National Laboratories is a multi-program laboratory managed and operated by Sandia Corporation, a wholly owned subsidiary of Lockheed Martin Corporation, for the U.S. Department of Energy's National Nuclear Security Administration under contract DE-AC04-94AL85000.

References

Bateman, V.I., Bell, R.G., Brown, F.A., Davie, N.T, M.A. Nusser, (1990). Evaluation of uniaxial and triaxial shock isolation techniques for a piezoresistive accelerometer," SAND90-1579C.

Cardillo, R.M., (1964). Dynamic testing of elastomer mountings, *Journal of Applied Polymer Science* 8: 53-71.

Chen, W. and Song, B., (2011). Split Hopkinson (Kolsky) bar. Design, testing and applications. Springer (New York).

Chu, A.S., (1988), Built-in mechanical filter in a shock accelerometer, *59th Shock and Vibration Symposium*. SAND88-2473C.

DeMarco, A.L., Chimich, D.D., Gardiner, J.C., Nightingale, R.W., Siegmund, G.P. (2010) The impact response of motorcycle helmets at different impact severities, *Accident Analysis and Prevention* 42: 1778-1784.

Frew, D.J., Akers, S.A., Chen, W., Green, M.L., (2010). Development of a dynamic triaxial Kolsky bar, *Measurement Science and Technology* 21(10): 1-10.

Kobayashi, H., Daimaruya, M., Nojima, T., Kajino, T., (2000). Effect of strain rate change during uniaxial dynamic tensile tests on instability strain, *Journal de Physique IV* 10: 433–438.

Kumar, A., Lok, T.S., and Pengjun, Z., (2004). Design of an impact striker for a split Hopkinson pressure bar, *Journal of the Institution of Engineers*, Singapore 4:119–130.

Lalanne, C., (2009), *Mechanical Vibration and Shock Analysis*, Wiley-ISTE.

Landro, L.D., Sala, G. Olivieri, D., (2002). Deformation mechanisms and energy absorption of polystyrene foams for protective helmets, *Polymer Testing* 21:217-228.

Li, X.B, Lok, T.S., Zhao, J. and Zhao, P.J., (2000). Oscillation elimination in the Hopkinson bar apparatus and resultant complete dynamic stress-strain curves for rocks, *International Journal of Rock Mechanics & Mining Science*, 37: 1055-1060.

Mercer, C.A. and Rees, P.L. (1971). An optimum shock isolator, *Journal of Sound and Vibration*, 18(4): 511-520.

Nelson, F.C., (1996). Vibration Isolation review: II. Shock Excitation, *Shock and Vibration*, 3(6); 451-459.

Othman, R. and Gary, G., (2007). Testing aluminum alloy from quasi-static to dynamic strain rates with a modified split Hopkinson bar method, *Experimental Mechanics* 47:295-299.

Park, K.S., Lim, S., Park, Y.P., Chang, Y.B., Park, N.C., (2012). Shock and vibration isolation of laptop hard disk drive using rubber mount, *Microsystems Technology* 18:1559-1566.

Sanborn, B., Song, B., Smith, S., (2016). Pre-strain effect on frequency-based impact energy dissipation through a silicone foam pad for shock mitigation, *Journal of Dynamic Behavior of Materials* 2:138-145.

Song, B. and Chen, W., (2004). Dynamic compressive behavior of EPDM rubber under nearly uniaxial strain conditions, *Journal of Engineering Materials and Technology* 126: 213-217.

Song, B. and Nelson, K., (2015). Dynamic characterization of frequency response of shock mitigation of a polymethylene diisocyanate (PMDI) based rigid polyurethane foam, *Latin American Journal of Solids and Structures* 12:1790-1806.

Song, B., and Chen, W., (2003). Dynamic compressive constitutive behavior of EPDM rubber, *Transactions of the ASME, Journal of Engineering Materials and Technology*, 125: 294-301.

Song, B., Chen, W., Yanagita, T., Frew, D.J., (2005). Confinement effects on the dynamic compressive properties of an epoxy syntactic foam, *Composite Structures* 67: 279-287.

Song, B., Connelly, K., Korellis, J., Lu, W.Y., Antoun, B.R., (2009). Improved Kolsky-bar design for mechanical characterization of materials at high strain rates, *Measurement Science and Technology*, 20:1-8.

Thorin, A., Azoug, A., Constantinescu, A., (2012). Influence of prestrain on mechanical properties of highly filled elastomers: measurement and modeling, *Polymer Testing* 31:978-986.

Yiannakopoulos, G and van der Schaaf P.J., (1998). Evaluation of accelerometer mechanical filters on submerged cylinders near an underwater explosion, *Shock and Vibration* 5: 255-265.

Yoon, S.H. and Kim, K.L., (2006). Passive low pass filtering effect of mechanical vibrations by a granular bed composed of microglass beads, *Applied Physics Letters* 89: 021906.

Zhao, H. and Gary, G., (1997). A new method for the separation of waves. Application to the SHPB technique for an unlimited duration of measurement, *Journal of the Mechanical Physics of Solids*, 45(7): 1184-1202.

Zhou, X.Y., Xia, K., Li, X.B., Li, H.B., Ma, G.W., Zhao, J., Zhou, Z.L., Dai, F., (2012) Suggested methods for determining the dynamic strength parameters and mode-I fracture toughness of rock materials, *International Journal of Rock Mechanics & Mining Science*, 49: 105-112.

Zou, L., Huang, K., Zhang, W., Rao, Y., Wang, L., (2011). Prestress rubber isolator and its mechanical properties, *Advanced Materials Research*, 163-167:4405-4414.